Journal of the European Ceramic Society **16** (1996) 1063–1073

PII: S0955-2219(96)00036-2
0955-2219/96/$15.00

Nanometric Si-Based Oxide Powders: Synthesis by Laser Spray Pyrolysis and Characterization

Nathalie Herlin, Xavier Armand, Emmanuel Musset, Hervé Martinengo, Michel Luce & Michel Cauchetier

CEA/DSM/DRECAM, Service des Photons, Atomes et Molécules, CE Saclay, 91191 Gif-sur-Yvette Cedex, France

(Received 13 December 1995; revised version received 22 January 1996; accepted 23 January 1996)

Abstract

The versatility of the laser synthesis method has been improved during the last few years. In this paper we present the synthesis of amorphous, nanosized Si/C/O powders obtained via ultrasonic injection of aerosol droplets into the beam of a high-power tunable CO_2 laser, using $(CH_3)_xSi(OC_2H_5)_{4-x}$ ($0 \leq x \leq 3$) and hexamethyldisiloxane as alkoxysilane precursors. All these precursors strongly absorb the CO_2 laser emission between 9 and 11 μm. The addition of precursors containing Al or Ti in tetraethoxysilane ($x = 0$) leads to Si,Al or Si,Ti oxide composite powders. The evolution of the powders (chemical composition, crystallization, morphology) during heat treatment under air, argon or nitrogen is studied by infra-red absorption, thermogravimetric analysis, transmission electron microscopy and X-ray diffraction. Silica powders with specific surface area up to 500 $m^2\ g^{-1}$ are obtained when heating in air. © *1996 Elsevier Science Limited.*

1 Introduction

Since the first experiments by Haggerty *et al.*,[1] a wide variety of ultrafine powders has been obtained by the laser synthesis method. An important application of these powders is structural ceramic technology. The synthesis method is based on the resonance between the emission of a CO_2 laser (10·6 μm) and the absorption of a gaseous precursor. It offers several advantages: due to the coherent laser beam, the chemical reaction zone is very well defined and there is no interaction with the reactor walls. This ensures extreme purity and very fine sized particles. However, the process has not been scaled up due to several limitations: the resonance condition clearly limits the precursor choice. To obtain Si-based powders the most common precursor is silane, which is an expensive and hazardous gas.

Recently, taking advantage of new technical developments, the versatility of the method has been improved. The ultrasonic injection of liquid precursors into the beam of the laser greatly extends the choice for the reactants. Moreover, it allows the use of cheaper and safer products. An example is given by the synthesis of Si/C/N powders.[2–4] Also, high power CO_2 lasers tunable between 9 and 11 μm are now available.[5]

To our knowledge, only two oxide powders TiO_2[6,7] and Al_2O_3[8] have been obtained by laser driven reactions in gaseous phases. The possibility to synthesize SiO_2 from an aerosol of tetraethoxysilane has already been reported.[9] In this paper we present the synthesis results obtained with different organosilicon precursors. Some nanosized silicon-based oxide powders have been synthesized using tetraethoxysilane and/or appropriate organometallic liquid precursors. Such powders may find applications in various fields. The organosilicon precursors are inexpensive, compared with silane, and after annealing treatments it is possible to obtain nanosized SiC powder as shown by Li *et al.*[10] for dimethyldiethoxysilane. The incorporation of fine carbon particles in silicon oxycarbide glasses (black glasses) has improved mechanical properties and chemical stability compared with silica.[11] In the field of catalysis there is an interest in incorporating fine metallic particles with good dispersion in high specific surface area silica.

In this paper, we report some preliminary characterization results and the evolution of these powders to silica, oxycarbide glasses or oxide composites after firing in air, argon or nitrogen between 600 and 1600°C.

2 Experimental

2.1 Procedure

The experimental device with aerosol generator, reaction chamber and powder collector has already been described.[2,9] A PRC-Oerlikon 1500-W, fast axial flow CO_2 laser has been modified to accept a grating which makes it tunable between 9 and 11 μm.[5]

The liquid organosilicon precursors with a variable O/Si atomic ratio and general formula $R_xSi(OR')_{4-x}$ where $0 \leq x \leq 3$, $R = CH_3$, $R' = C_2H_5$ and hexamethyldisiloxane $[(CH_3)_3SiOSi(CH_3)_3]$ were supplied by Fluka Chemie A.G. or Sigma–Aldrich Chimie and used without further purification. Table 1 presents the different precursors with their chemical formulae: $x = 0$ corresponds to tetraethoxysilane $Si(OC_2H_5)_4$, $x = 1$ corresponds to triethoxymethylsilane $(CH_3)Si(OC_2H_5)_3$, $x = 2$ corresponds to diethoxydimethylsilane $(CH_3)_2Si(OC_2H_5)_2$ and $x = 3$ corresponds to ethoxytrimethylsilane $(CH_3)_2Si(OC_2H_5)_2$.

Some of these precursors have been used in the preparation of Si/C/O oxycarbide glasses, carbon–SiO_2 glass composites or SiC by the sol–gel process.[12–16] Recently, vaporized diethoxydimethylsilane has been irradiated with the focused beam of a high-power fixed-frequency CO_2 laser for SiC formation.[10] These precursors have been chosen because they absorb infra-red radiation in the 9–11 μm region corresponding to Si–O–C or Si–O–Si bonds. Weaker absorption bands appear near 10·6 μm for $0 \leq x \leq 3$ (see Table 1). Figure 1 presents the absorption lines of the different liquid precursors and the emission lines of the tunable CO_2 laser, showing that the resonance condition is easily achieved for this family of precursors.

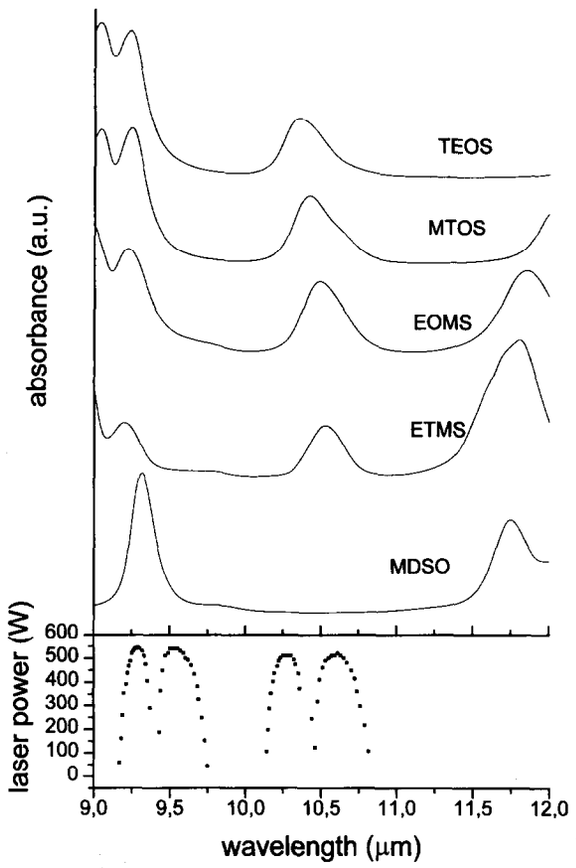

Fig. 1. Absorption spectra of the different precursors and emission lines of the laser at half discharge current (i = 30 mA).

Composite precursors were obtained by mixing liquid titanium propoxide — $Ti(OC_3H_7)_4$ — or solid aluminium isopropoxide — $Al(OCH(CH_3)_2)_3$ — with tetraethoxysilane. The Ti/Si and Al/Si atomic ratios are equal to 0·1 in the liquid phase.

The aerosols were produced by an ultrasonic spraying technique (Pyrosol process) which has been widely used in thin layer deposition.[17] The aerosol characteristics (such as droplet size and flow rate) depend on the liquid properties (viscosity, surface tension, volatility). The size of the aerosol droplets is given by:

$$d = \left(\frac{\pi \sigma}{4\rho f^2}\right)^{1/3}$$

where σ and ρ are the surface tension and density of the liquid respectively, and f is the frequency of the transducer (800 kHz). Using measured or calculated σ values,[18–20] the size of the droplets can be calculated for the different precursors: they are in the range 2·8–3·0 μm.

Table 1 summarizes some properties of the precursors used and laser irradiation conditions. The aerosol droplets are carried out in an argon flow through a 13 mm diameter nozzle into the reaction chamber. In order to keep the residence time in the laser beam (i.e. the reaction time) constant, the argon flow was fixed to 1280 $cm^3\ min^{-1}$. The droplets intersect the laser beam (12 mm diameter) orthogonally with an incident power in the 350–400 W range (discharge current = 30 mA). Powders are collected in a glass chamber located between the reaction cell

Table 1. List of precursors and irradiation conditions

	Precursor	*Molecular weight (g)*	*Density of precursor (g cm^{-3})*	*Boiling point (°C)*	*Sample designation*	*Laser power (W)*	*Absorbed power (W)*	*Wavelength (μm)*
Tetraethoxysilane	$Si(OC_2H_5)_4$	208·3	0·934	165·8	TEOS	400	220–250	9·293
Triethoxymethylsilane	$(CH_3)Si(OC_2H_5)_3$	178·3	0·896	143	TEMS	430	220–250	9·293
Diethoxydimethylsilane	$(CH_3)_2Si(OC_2H_5)_2$	148·3	0·840	114–115	EOMS	420	280–290	9·260
Ethoxytrimethylsilane	$(CH_3)_3Si(OC_2H_5)$	118·3	0·757	75–76	ETMS	420	330–350	9·293
Hexamethyldisiloxane	$(CH_3)_3SiOSi(CH_3)_3$	162·4	0·759	99–101	MDSO	345	260–280	9·488
Tetraethoxysilane+ aluminium isopropoxide	0·9 $Si(OC_2H_5)_4$ + 0·1 $Al(OC_3H_7)_3$	204·25	1·035	solid	AlTEOS	440	290–310	9·293
Tetraethoxysilane + tetrapropylorthotitanate	0·9 $Si(OC_2H_5)_4$ + 0·1 $Ti(OC_3H_7)_4$	284·26	0·965	170/400 Pa	TiTEOS	430	280–300	9·293

and the vacuum pump. The typical duration of an experiment is 40 min.

2.2 Characterizations

Chemical analyses were achieved by conventional methods (CNRS analysis laboratory) as previously presented.[2] The relative uncertainty is equal to ± 2% for C and O, ± 3% for Si, Ti and Al. The heat treatments were carried out either dynamically by thermo- gravimetric analysis (TGA) in flowing air, argon or nitrogen, or statically in a Nabetherm HT08/1750 oven for oxidation in air or in a Pyrox GE80 graphite furnace for annealing in argon and nitrogen. The heating rate was 10°C min^{-1} and the dwell time 1 h.

X-ray diffraction (XRD) patterns of the crystalline phases were obtained with an automated powder diffractometer (Philips, APD 1700) using CuK_α radiation. Information on chemical bonding was obtained by infra-red (IR) spectrophotometry (Perkin–Elmer 580 spectrophotometer) in the 4000–400 cm^{-1} range using the KBr pellet technique. The specific surface areas were measured by the BET method using a Micromeretics Flowsorb 2300. The morphology was studied by transmission electron microscopy (TEM) (CM20 Philips).

3 Results and Discussion

3.1 Si/C/O powders

During laser pyrolysis a wide yellow flame is observed in the reaction zone. The production rate is rather low, from 8 to 27 g h^{-1}, but no effort has been made to optimize this. It is correlated with the weight of displaced precursor and is very close to our first results obtained in Si/C/N composite powder synthesis from laser pyrolysis of a hexamethyldisilazane aerosol.[2] As shown in Table 1, the absorbed laser power — in the range 50 to 80% of the incident power — is high compared with the absorption in gaseous laser-driven reactions, e.g. 10% for SiC synthesis.[21] A partial explanation is given by the power excess necessary to vaporize the liquid droplets. Table 1 also presents the abbreviations used in the following sections for the samples synthesized from the different precursors.

3.1.1 As-produced powders

In all cases the as-produced powders are black and amorphous as confirmed by XRD. Table 2 gives the chemical elemental analysis (wt%) of the produced powders together with the chemical composition of the reactive phase. An empirical chemical composition of the powders is also presented. The chemical composition of the powders is a function of the chemical composition of the reactive phase. The O and Si content is higher in the powder than in the precursor. The relative evolution is similar for all the chemical elements: for example, O content in the powders decreases when it decreases in the precursor. A more precise comment taking into account the nature of the chemical bond is presented in the following.

The TEM micrographs show that all the powders consist of round particles with low size dispersion. The particles stick together in a chain-like manner. Figure 2 presents micrographs of EOMS and TEOS samples, with a smaller grain size (≈ 20 nm) for the EOMS sample compared with all other samples (>30 nm). These observations are in agreement with BET measurements (Table 2). TEM micrographs at higher magnification show that most of the particles are slightly agglomerated and can be dispersed, but in some cases there is a strong connection between the particles. Also, some ribbons (similar to carbon ribbons) are present in all the samples. As an example, Fig. 2(a) presents the ribbons observed in a TEOS sample.

Table 2 shows no clear correlation between the BET surface of as-formed powders and the experimental synthesis conditions (such as size of the droplets, laser power and argon flow). One can see that for $R_xSiR'_{4-x}$, $x = 1$ to 3, the specific surface area decreases with increasing x.

Figure 3 presents the IR spectra of as-formed powders. The TEOS sample corresponds to pure amorphous silica (opaline type).[22,23] The peaks at 1100 and 810 cm^{-1} correspond to antisymmetric Si–O–Si stretching and the peak at 470 cm^{-1} corresponds to the Si–O–Si bending mode.[24] This

Table 2. Chemical analysis of precursors and as-formed produced powders

Precursor	*wt%*					*Samples*	*wt%*					*Equivalent chemical formula*	S_{BET} ($m^2 g^{-1}$)
	C	*O*	*Al*	*Ti*	*Si*		*C*	*O*	*Al*	*Ti*	*Si*		
$Si(OC_2H_5)_4$	46·1	30·7			13·4	TEOS	21·1	41·8			35·1	$SiO_{2.08}C_{1.40}$	133
$(CH_3)Si(OC_2H_5)_3$	47·1	26·9			15·7	MTOS	27·0	36·6			32·4	$SiO_{1.98}C_{1.94}$	228
$(CH_3)_2Si(OC_2H_5)_2$	48·5	21·6			18·9	EOMS	28·3	34·0			35·3	$SiO_{1.68}C_{1.87}$	210
$(CH_3)_3Si(OC_2H_5)$	50·7	13·5			23·7	ETMS	29·4	28·3			42·4	$SiO_{1.17}C_{1.62}$	133
$(CH_3)_3SiOSi(CH_3)_3$	44·3	9·8			34·5	MDSO	29·9	16·7			50·7	$SiO_{0.58}C_{1.38}$	70
$Si(OC_2H_5)_4$+ $Al(OCH(CH_3)_2)_3$	46·7	30·0	1·2		12·2	AlTEOS	19·2	43·8	3·6		33·8		84
$Si(OC_2H_5)_4$+ $Ti(OC_3H_7)_4$	46·6	29·7		2·0	11·8	TiTEOS	23·2	40·6		5·9	31·1		70

observation is in good agreement with the chemical composition of the powder: the O/Si atomic ratio is equal to 2·09, very close to the ratio of pure silica. The absorption lines of amorphous silica powders are observed in all spectra. In the MTOS sample, a new feature at 1260 cm^{-1} appears. This corresponds to a Si–CH_3 bond and is correlated with the presence of Si–CH_3 in the precursor. It is attributed to partially dissociated precursor remaining trapped in the powder. The peak is very weak, indicating that a very small part of the precursor remains in the powders. In TEOS and EOMS samples C atoms do not seem bonded to Si or O, suggesting the presence of an abundant phase composed of free carbon in good agreement with the presence of carbon ribbons observed by TEM. The samples MTOS, EOMS, ETMS and MDSO are produced from precursors containing an increasing number of Si–C bonds compared with Si–O bonds. The infra-red spectra show an increasing contribution of the feature located at 870 cm^{-1}, which is attributed to the Si–C bond.

From the TEM micrographs, the IR spectra and using the empirical chemical composition, it can be assumed that the samples are mainly composed of silica, silicon carbide and free carbon with different ratio (Table 3). These compositions are in good agreement with the relative intensities of SiC and SiO_2 observed in IR spectra. Also, this composition (SiC bonds) is related to the number of SiC bonds in the liquid precursor (Fig. 4). However, IR spectra alone do not enable any conclusions to be drawn about the local environment. As already observed for Si/C/O samples obtained by other methods (see, for example, Ref. 11), we think that in all our samples we have a distribution of SiO_xC_{4-x} tetrahedra. The local environment around Si and C atoms will be investigated more closely by nuclear magnetic resonance spectroscopy. The nature of the C excess, designated here as free carbon, should be clarified using (for example) Raman spectroscopy.

The powders obtained by irradiation of vaporized diethoxydimethylsilane with the focused beam of a

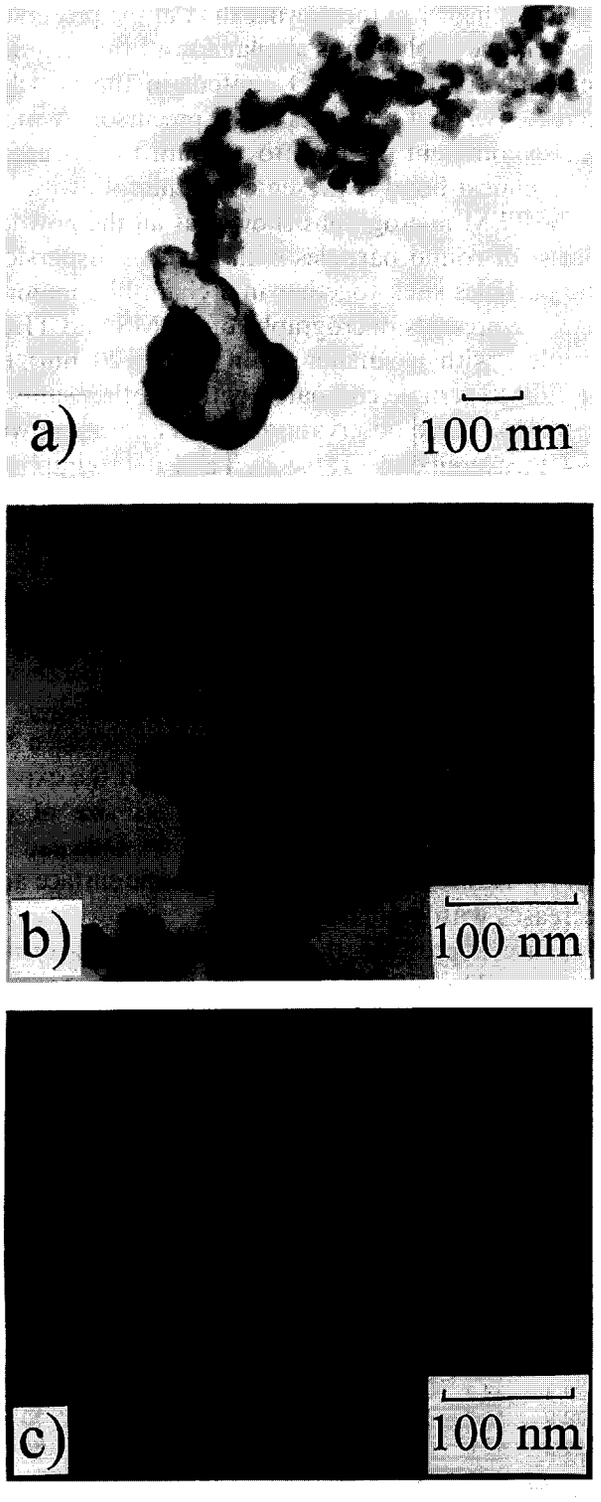

Fig. 2. TEM micrographs of as-formed TEOS (a,b) and EOMS (c) samples.

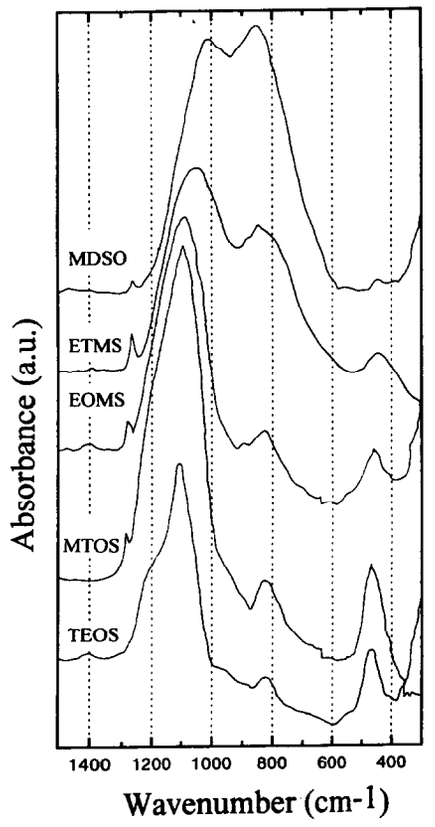

Fig. 3. IR spectra of as-formed Si/C/O powders.

Table 3. Assumed chemical composition of powders, calculated and measured weight evolution with oxidation

Sample	*Composition*	*Δm/m (%) [calculated]*	*Δm/m (%) [measured]*
TEOS	SiO_2 +1·4 C	−22	−21·8
MTOS	SiO_2 +1·94 C	−28	−28·4
EOMS	SiO_2 + 0·19 SiC + 2·03 C	−22	−21·8
ETMS	SiO_2 + 0·71 SiC + 2·05 C	−1	−7·8
MDSO	SiO_2 + 2·45 SiC + 2·30 C	+11	+12·2

high-power fixed-frequency CO_2 laser[10] can be compared with the EOMS sample. The grain size in each sample is of the same order of magnitude. The powders are amorphous. The chemical analysis shows that the EOMS sample is more oxidized (34/25 wt%). This result can be related to the different experimental conditions, in particular the laser power density is much lower in the present work: 100 W cm^{-2} compared with 5100 W cm^{-2} in Ref. 10.

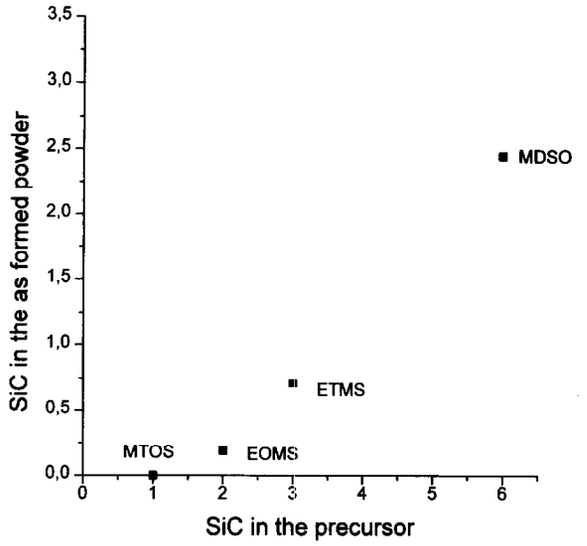

Fig. 4. Number of SiC bonds in the produced powders as a function of SiC bonds in the precursor.

3.1.2 Annealed powders

3.1.2.1 Annealing in air. Figure 5 presents TGA curves of Si/C/O samples after heating to 1600°C in air. The weight evolution shows a very different behaviour, correlated with the chemical composition of the sample. Assuming that annealing under air leads to complete oxidation of the different compounds of the powders and using the chemical composition of Table 3, two mechanisms are involved:

$$SiO_2 + \text{free C} + O_2 \rightarrow SiO_2 + CO_2 \quad (1)$$

$$SiO_2 + SiC + O_2 \rightarrow SiO_2 + CO_2 \quad (2)$$

It is easy to calculate the weight changes due to oxidation for the different samples. The result is presented in Table 3. The calculations are compared with the experimental results (Fig. 5). For TEOS and MTOS samples, the loss is attributed to oxidation of free carbon. The weight loss is of the same order of magnitude as the C content in the as-formed powders (Table 2). For other samples, there is a

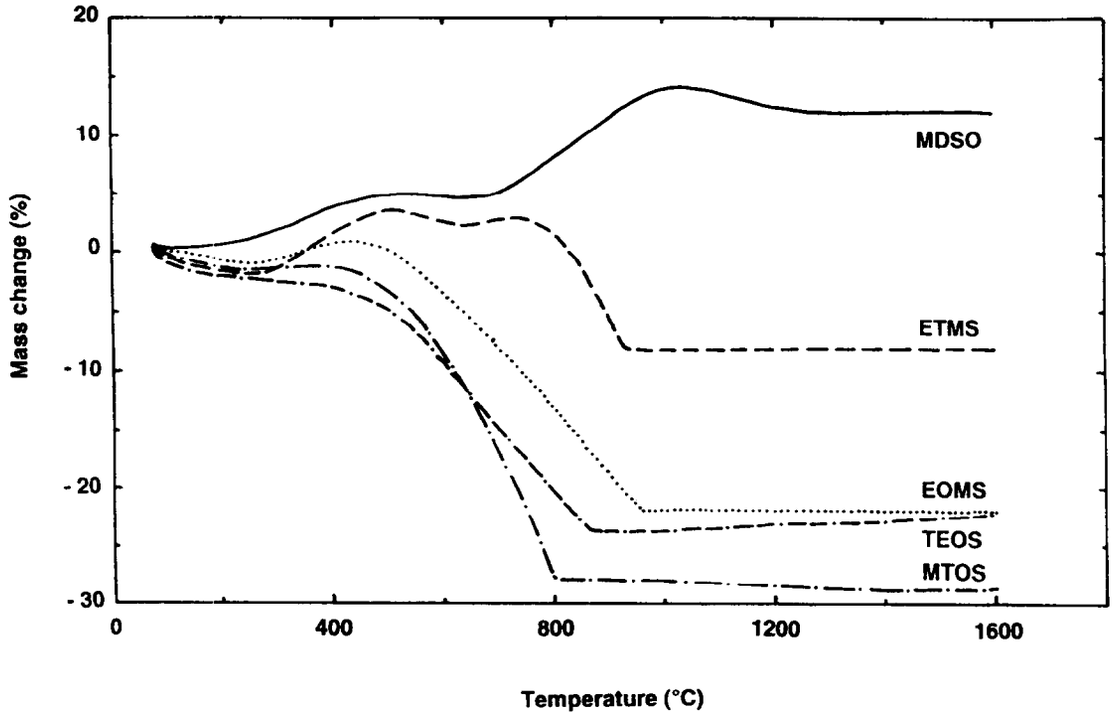

Fig. 5. TGA curves of Si/C/O powders fired under air up to 1600°C (heating rate 10°C min^{-1}, dwell time: 1 h).

competition between weight loss due to reaction (1) and gain due to reaction (2). For all samples the qualitative agreement is good between calculations and experimental measurements, which is a confirmation that the assumed mechanisms are dominant.

After heating for 3 h at 600°C under air, the chemical analysis shows that the C content is very weak (<0·5%) for all samples except MDSO, and the powders turn white. The chemical composition is already very similar to that of silica. For sample MDSO, after 3 h of heating at 600°C under air, the weight increases by 12% and the C content is still 14% because it is not so easy to oxidize C bonded to Si as compared with free C, as already shown in laser synthesized SiC powders.[25] IR spectra of annealed powder show the presence of SiC and SiO bonds, with a decreasing contribution of SiC compared with the as-formed powder. At higher temperature the 870 cm^{-1} absorption band of SiC disappears and the C content becomes negligible. All these observations are in good agreement with reactions (1) and (2).

Figure 6 shows that the specific surface area increases markedly after annealing at 600°C for samples with $x = 0$ to 3 and then decreases at higher temperatures. A value near 500 $m^2\ g^{-1}$ is measured for the MTOS sample. At 600°C TEM observations show no change in the morphology or size of the powders, grain growth begins around 900°C correlated with the decreasing specific surface area. The increase in specific surface area is thus attributed to an increased porosity due to the departure of C atoms. Porosity and density measurements are necessary to confirm this hypothesis. For the MDSO sample, the specific surface area is not as significantly modified at 600°C as it is in the other compounds. In this latter case, oxidation leads to a less porous material. MTOS sample is of special interest because the surface area is still very high at 900°C (273 $m^2\ g^{-1}$). At 1300°C, the specific surface area is below 1 $m^2\ g^{-1}$ for all samples, indicating high densification.

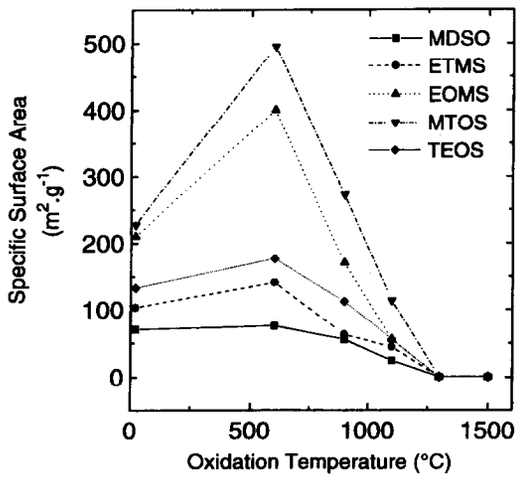

Fig. 6. Evolution of the specific surface area of Si/C/O powders with oxidation temperature.

Figure 7 presents the evolution of IR spectra of the TEOS sample after heat treatments under air at different temperatures, the general trend is identical for all the samples. After 1 h of heating at 600°C, the feature attributed to $Si–CH_3$ disappears from the IR spectra. The IR spectra still exhibit the characteristic features of opaline up to 1200°C. At this temperature, TEOS and EOMS samples are still amorphous as confirmed by XRD. The O/Si (wt) ratio is very close to 1·14 (pure silica) and the C content is about

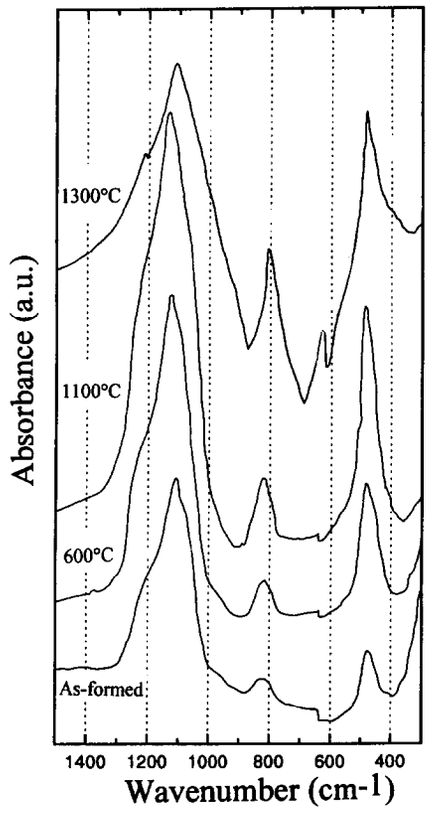

Fig. 7. Evolution of IR spectra of TEOS after annealing under air.

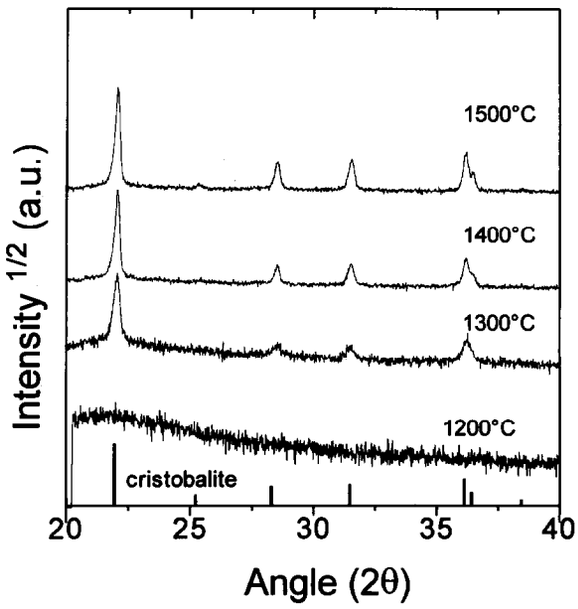

Fig. 8. Evolution of XRD patterns of TEOS.

≅ 100 ppm. After heat treatment in air at 1300°C, TEOS sample crystallizes as shown in Fig. 8. EOMS sample is also crystallized at this temperature. The cristobalite structure is identified through IR and XRD (JCPDS no. 39-1425) (Figs 7 and 8), which corresponds to the chemical analysis. A new peak at 620 cm^{-1} appears in the IR spectra (Fig. 7), characteristic of the cristobalite structure.[22,23] The broad structure between 1000 and 1300 cm^{-1} splits into two bands at 1100 and 1200 cm^{-1}, which correspond to the longitudinal and transverse mode of the SiO_2 lattice. This indicates a long-range crystalline order.[26]

Above 1300°C, the XRD patterns of TEOS sample show an increasing crystallite size with increasing temperature.

At 1300°C, MDSO sample is still amorphous under XRD. The cristobalite structure is identified after heat treatment at 1400°C, and the chemical analysis gives the composition of silica O/Si = 1·15 (wt).

3.1.2.2 Annealing under argon and nitrogen. Heat treatment in argon was performed at 1300°C, which is before the thermal reaction of silica (carboreduction), and at 1500°C after the carboreduction. Annealing under nitrogen was performed at 1500°C. At this temperature, nitrogen becomes active for nitridation. IR spectra of annealed powders are shown in Figs 9 and 10.

Under argon at 1300°C [Fig. 9(a)] the IR spectrum of the TEOS sample is very similar to that of silica. In the other spectra mixtures of silica and silicon carbide appear, the silicon carbide content increasing from MTOS to MDSO sample as shown by the change in relative intensities of IR bands at 1100 cm^{-1} for SiO_2 and at 870 cm^{-1} for SiC. At 1500°C [Fig. 9(b)] only IR bands of SiO_2 appear for the TEOS sample. In the other samples SiC is the dominant compound, with the IR band at 870 cm^{-1}. The pronounced dip near 1000 cm^{-1} was observed previously[2,27,28] and is generally related to the size increase obtained by the coalescence of particles following the carboreduction of silica.

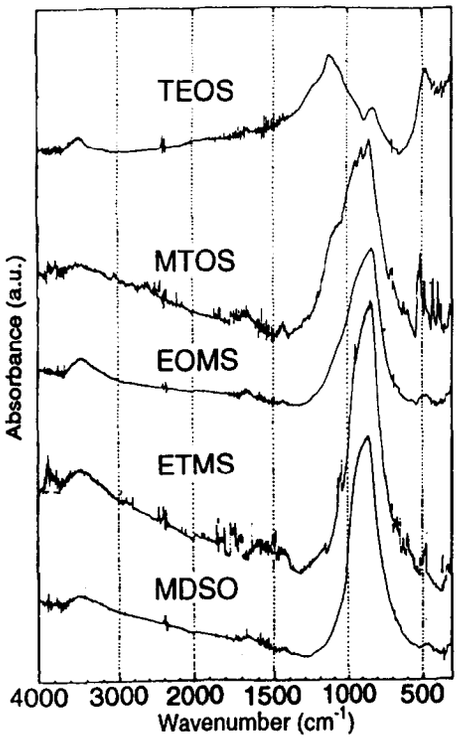

Fig. 10. IR spectra of Si/C/O powders after annealing under nitrogen at 1500°C.

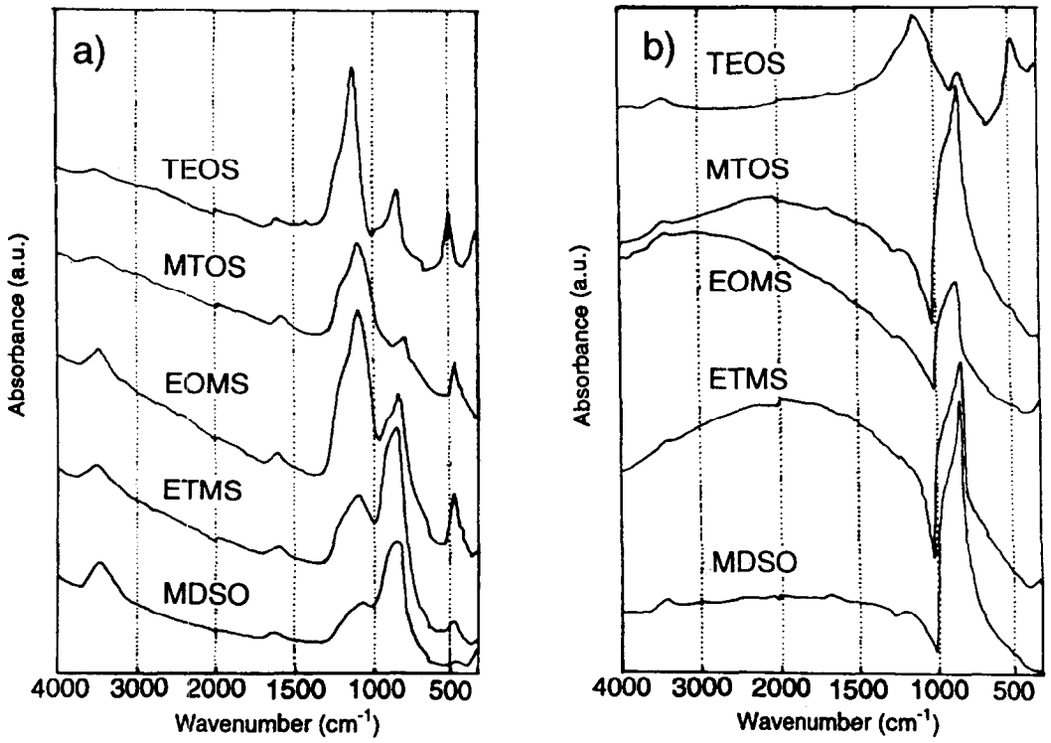

Fig. 9. IR spectra of Si/C/O powders after annealing under argon at 1300°C (left) and 1500°C (right).

IR spectra of the nitrided powders (Fig. 10) show differences relating to the initial sample. The IR spectrum of the TEOS sample is quite similar to the SiO_2 spectrum. In the other spectra, IR bands due to crystallized Si_3N_4 appear in the 500–400 cm^{-1} region.

Tables 4 and 5 present the characterizations and the chemical compositions of these powders. They show a good agreement with the IR results.

At 1500°C, under argon or nitrogen, coalescence of TEOS sample particles occurs promptly when the spe- cific surface area is decreased below 1 $m^2\ g^{-1}$ (Table 4). The remaining C content is low (about 2·5 wt%) and the nitridation under nitrogen is negligible (0·9 wt% N). The calculated chemical composi-tion (Table 5) shows silica as the predominant phase. The weight loss can be explained by $SiO_2 + C \rightarrow SiO\uparrow + CO\uparrow$ with SiO and CO volatilizations. The carbo-reduction reaction of the silica can be neglected for annealing under N_2. The non-nitridation of the TEOS sample appears to be different from result relating to the preparation of Si_3N_4 from alkoxide-derived oxides by carbothermal reduction and nitridation.[29]

In the other samples the C content after annealing at 1500°C under argon remains high (25–30 wt%) and the O content decreases below 10 wt%, relating to the carboreduction of the silica and the formation of silicon carbide. Similar high weight losses (Table 4) — up to 80 wt% — have been observed in the preparation of silicon carbide from organosilicon gels.[16,30,31] At 1300°C, XRD patterns show that the MDSO sample is slightly crystallized and the β-SiC structure is identified (JCPDS no. 29-1129). At higher temperature the crystallite size increases. The evolution of specific surface area shows that the nanometric structure is conserved up to 1300°C. As in the previous case, the specific surface area of the MTOS sample is quite high: 242 $m^2\ g^{-1}$.

Annealing under nitrogen at 1500°C leads to a very efficient nitridation for these samples. The N content seems related to the initial specific surface area of the samples and decreases from 24·1 to 11·0 wt% when the specific surface area decreases from 230 to 70 $m^2\ g^{-1}$ (Table 2). The corresponding Si_3N_4 content in the remaining powder is high, up to 60 wt% for MTOS sample (Table 5). The nitridation of the EOMS sample appears as different from results of Ref. 10, where the heat treatment under nitrogen at 1600°C leads to crystalline SiC containing 6 wt% of oxygen.

3.2 Titanium- and aluminium-doped silica powders

3.2.1 As-formed powders

Table 2 shows that the Al/Si and Ti/Si ratios are equal in the reactive phase and in the powders, which is interesting when it is intended to produce composites with controlled chemical composition. Figure 11 presents the IR spectra of as-formed powders compared with the spectrum of the pure TEOS sample. In TiTEOS, the absorption at 950 cm^{-1} is attributed to Si–O–Ti modes of vibration. No feature that could be attributed to a pure TiO_2 phase can be observed. In the AlTEOS sample, there is no specific feature that could be related to the presence of Al. In both cases, pure amorphous silica is identified.[22,23] It seems that the incorporation

Table 4. Characterizations of Si/C/O powders after annealing under argon and nitrogen

	Ar, 1300°C, 1 h				*Ar, 1500°C, 1 h*				*N_2, 1500°C, 1 h*				
	C (wt%)	O (wt%)	Δm (%)	S_{BET} ($m^2\ g^{-1}$)	C (wt%)	O (wt%)	Δm (%)	S_{BET} ($m^2\ g^{-1}$)	C (wt%)	O (wt%)	N (wt%)	Δm (%)	S_{BET} ($m^2\ g^{-1}$)
TEOS	16·0	39·7	n.m.	85	2·5	53·6	−22·9	0·1	2·4	49·3	0·9	−19·5	0·2
MTOS	26·5	34·7	−24·1	242	26·6	8·6	−74·1	88	10·3	n.m.	24·1	−62·0	101
EOMS	25·5	32·7	−30·0	173	28·8	n.m.	−75·0	20	11·7	n.m.	23·5	−60·4	70
ETMS	26·9	21·5	−24·8	102	29·3	4·8	−49·3	25·5	20·1	6·7	13·4	−38·2	86
MDSO	28·8	15·5	−38·0	70	27·5	5·3	−33·7	36·5	20·4	5·9	11·0	−2·4	58

n.m.: not measured

Table 5. Chemical composition (in wt%) of Si/C/O powders after annealing under argon and nitrogen

	Ar, 1300°C, 1 h			*Ar, 1500°C, 1 h*			*N_2, 1500°C, 1 h*			
	SiO_2	SiC	C	SiO_2	SiC	C	SiO_2	Si_3N_4	SiC	C
TEOS	74·4	13·7	11·9	97·5	0	2·5	92·6	2·3	3·9	1·2
MTOS	65·2	11·9	22·9	16·2	69·4	5·8	n.c.	60·5	n.c.	n.c.
EOMS	61·5	18·7	19·9	n.c.	n.c.	n.c.	n.c.	58·9	n.c.	n.c.
ETMS	40·3	46·8	12·9	9·0	88·1	2·9	12·6	33·6	47·7	6·1
MDSO	29·1	59·0	11·1	10·0	89·1	0·8	11·1	27·4	58·7	2·8

n.c.: not calculated

of a second phase is related to a decrease of the specific surface: 133, 84 and 70 $m^2 g^{-1}$ for TEOS, AlTEOS and TiTEOS samples, respectively.

3.2.2 Annealed powders (under air)

3.2.2.1 Titania-silica composite. After heat treatment at 600°C the weight loss of the TiTEOS sample is 25%, which corresponds to the C content in the as-formed powder (Table 2). As in the case of TEOS, the weight loss is attributed to the oxidation of free C [reaction (1)]. The Si/Ti ratio is not modified by oxidation up to 1300°C. Figure 12 presents the XRD patterns of TiTEOS samples as a function of heat treatment. It shows that crystallization begins between 600 and 900°C. At 900°C, two different TiO_2 phases [anatase (JCPDS no. 21-1272) and rutile (JCPDS no. 21-1276)] are present simultaneously. At 1200°C, the dominant features are attributed to rutile. A beginning of silica crystallization into the cristobalite phase is observed, also seen on IR spectra (Fig. 13). At this temperature, pure silica obtained from TEOS is still amorphous. At 1400°C anatase has disappeared, cristobalite and rutile appear well crystallized.

In the IR spectra of TiTEOS (Fig. 13) only the peak at 950 cm^{-1}, already attributed to Si–O–Ti, is added to the pure silica spectra and there is no modification of this band with temperature. No band of pure TiO_2 can be observed.

The specific surface area evolution is similar to the specific surface area evolution of the TEOS sample, with a maximum value of 137 $m^2 g^{-1}$.

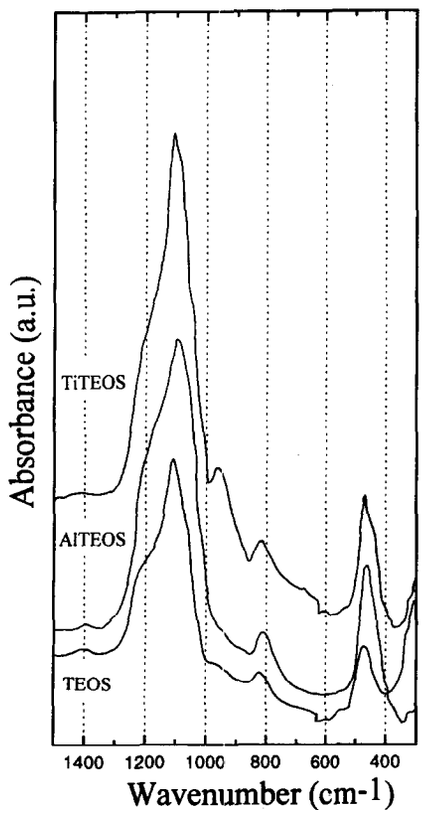

Fig. 11. IR spectra of as-formed Al and Ti (composite) powders.

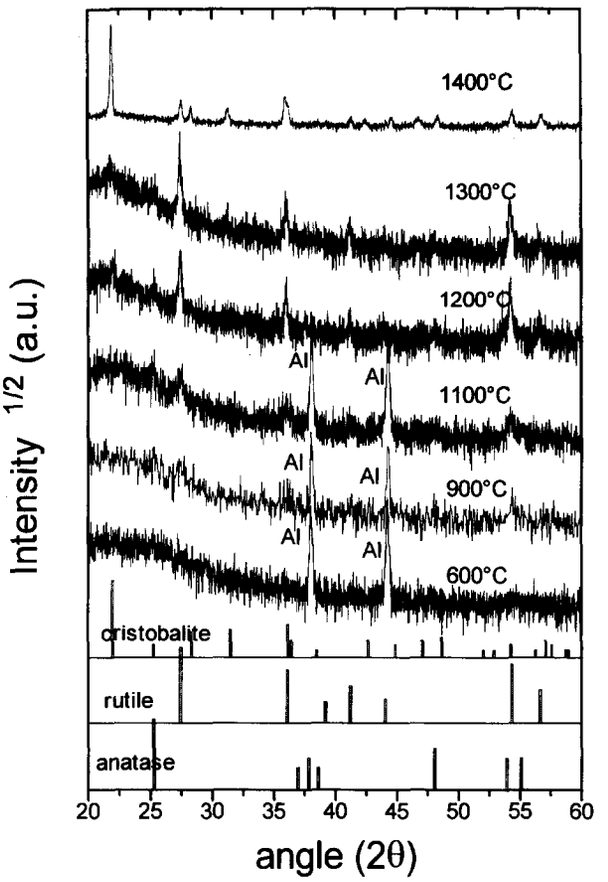

Fig. 12. Evolution of XRD patterns of TiTEOS sample as a function of oxidation temperature.

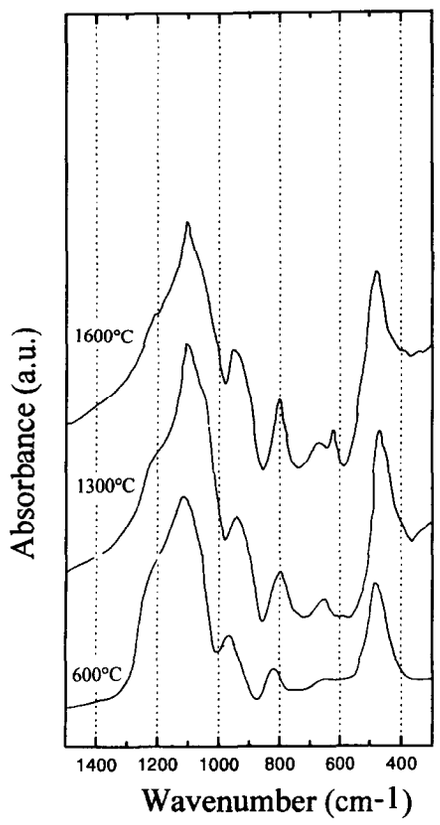

Fig. 13. Evolution of IR spectra of TiTEOS sample as a function of oxidation temperature.

3.2.2.2 Alumina–silica composite. After heat treatment at 600°C the weight loss of the AlTEOS sample is 17%, comparable with the C content in the as-formed powder (Table 2). As in the former case, weight loss is explained by reaction (1). Figure 14 presents the evolution of IR spectra as a function of annealing temperature. It is not possible to identify any line of pure alumina Al_2O_3 in these spectra. Only a line at 880 cm^{-1} is different from the silica spectra, it becomes a clear structure in the spectra at 1600°C and is usually attributed to Si–O–Al bonds.[35] XRD patterns presented in Fig. 15 show that the crystallization begins at 1200°C and cristobalite is identified, in good agreement with IR spectra. Another crystallized phase containing Al is present; it is not clear whether it is sillimanite or mullite, both of them being mixed phases composed of SiO_2 and Al_2O_3.[36]

4 Conclusion

In this paper we have shown that it is possible to produce amorphous, nano-sized, silicon-based oxide powders by laser–aerosol interaction. Silica powders with high specific surface area have been obtained. The incorporation of metallic elements (Al,Ti) in the powder is quite easy. In a first step, the evolution of the structure of the as-formed amorphous powders has been studied as a function of heat treatments using conventional characterization methods. The results concern long-range order and mainly the bulk.

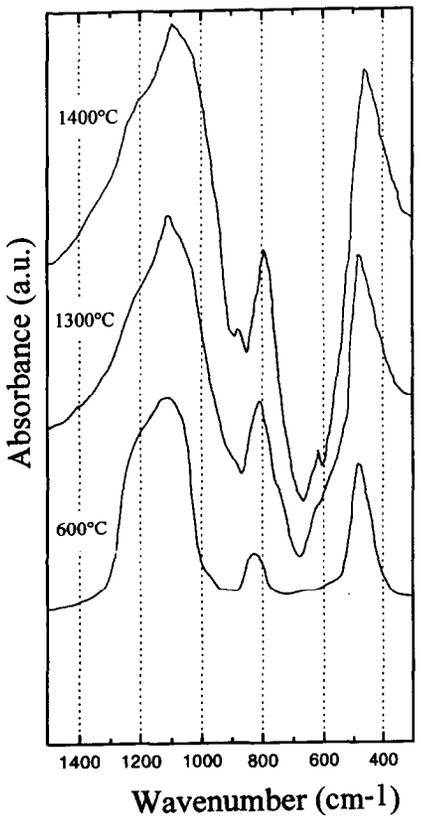

Fig. 14. Evolution of IR spectra of AlTEOS sample as a function of oxidation temperature.

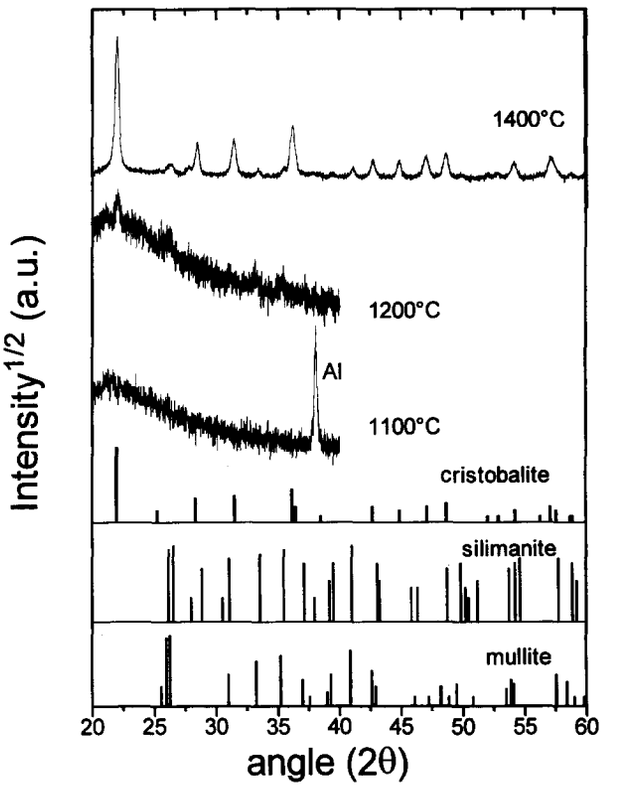

Fig. 15. Evolution of XRD patterns of AlTEOS sample as a function of oxidation temperature.

In the future, it seems important to characterize the microstructure and the short-range order to correlate these with the properties of the material (sintering behaviour). In particular, it would be interesting to clarify the C bonding and the role of free carbon in the evolution of specific surface area and reactivity.

New experiments are in progress to synthesize silica containing different amounts of C, Al, Ti or other metallic elements by adjusting the process parameters. The possibility of synthesizing a mixture of different phases with controlled chemical composition and good dispersion seems very promising, in particular for the production of heterogeneous catalysts. Work is in progress to compare the properties of such powders with properties of powders obtained by other methods.

Acknowledgements

The authors are very grateful to Mrs C. Robert and Mr H. Lathus from CEA-CEREM for performing the thermogravimetric analyses and high-temperature oxidation experiments, respectively.

References

1. Cannon, W. R., Danforth, S. C., Flint, J. H., Haggerty, J. S. & Marra, R. A., Sinterable ceramic powders from laser driven reactions. I. Process description and modeling. *J. Am. Ceram. Soc.*, **65**[7] (1982) 324–329.
2. Cauchetier, M., Croix, O., Herlin, N. & Luce, M., Nanocomposite Si/C/N powder production by laser–aerosol interaction. *J. Am. Ceram. Soc.*, **7**[4] (1994) 993–998.

3. Herlin, N., Musset, E., Luce. M. & Cauchetier, M., Synthesis of nanocomposite Si/C/N powders by laser spray pyrolysis of hexamethyldisilazane. *J. Eur. Ceram. Soc.*, **13**[2] (1994) 285–291.
4. Musset, E., Herlin, N., Cauchetier, M. & Luce, M., Nanometric Si/C/N composite powders elaboration by laser–aerosol interaction. *J. Aerosol Sci.*, **25**[7] (1994) 1364.
5. Whitehouse, D., Tullio, K. & Thomson, A., Industrial, kilowatt-class, tunable CO_2 laser. In *Laser Materials Processing*, Proceedings of ICALEO (Orlando, FL, 25–29 Oct. 1992). Laser Institute of America, Vol. 75, pp. 42–52.
6. Casey, J. D. & Haggerty, J. S., Laser-induced vapour phase synthesis of titanium dioxide. *J. Mater. Sci.*, **22**[12] (1987) 4307–4312.
7. Curcio, F., Musci, M., Notaro, M. & Quattroni, G., Laser induced synthesis of ultrafine TiO_2 powders. In *Ceramics Today — Tomorrow's Ceramics*, ed. P. Vincenzini. Materials Science Monographs 66D, Elsevier, Amsterdam, The Netherlands, 1991, pp. 2569–2578.
8. Borsella, E., Botti, S., Giorgi, R., Martelli, S., Turtu, S. & Zappa, G., Laser-driven synthesis of nanocrystalline alumina from gas phase precursors. *Appl. Phys. Lett.*, **63**[10] (1993) 1345–1347.
9. Luce, M., Herlin, N., Musset, E. & Cauchetier, M., Laser synthesis of nanometric silica powders. *NanoStruct. Mater.*, **4**[4] (1994) 403–408.
10. Li, Y., Liang, Y., Zheng, F. & Hu, Z., Carbon dioxide laser synthesis of ultrafine silicon carbide powders from diethoxydimethylsilane. *J. Am. Ceram. Soc.*, **77**[6] (1994) 1662–1664.
11. Soraru, G., Silicon oxycarbide from gels. *J. Sol–Gel Sci. Technol.*, **2** (1994) 843–848.
12. Babonneau, F., Thorne, K. & Mackenzie, J. D., Dimethyldiethoxysilane–tetraethoxysilane copolymers: precursors for the Si–C–O system. *Chem. Mater.*, **1**[5] (1989) 554–558.
13. Bois, L., Maquet, J., Babonneau, F., Mutin, H. & Bahloul, D., Structural characterization of sol–gel derived oxycarbide glasses. 1. Study of the pyrolysis process. *Chem. Mater.*, **6**[6] (1994) 796–802.
14. Babonneau, F., Hybrid siloxane–oxide materials via sol–gel processing: structural characterization. *Polyhedron*, **13**[8] (1994) 1123–1130.
15. Kamiya, K., Yoko, T., Sano, T. & Tanaka K., Distribution of carbon particles in carbon/SiO_2 glass composites made from $CH_3Si(OC_2H_5)_3$ by the sol–gel method. *J. Non-Cryst. Solids*, **119**[1] (1992) 14–20.
16. Hatakeyama, F. & Kanzaki, S., Synthesis of monodispersed spherical β-silicon carbide powder by a sol–gel process. *J. Am. Ceram. Soc.*, **73**[7] (1990) 2107–2110.
17. Langlet, M. & Joubert, J. C., The pyrosol process or the pyrolysis of an ultrasonically generated aerosol. In *Chemistry of Advanced Materials*, ed. C. N. R. Rao. Blackwell Scientific Publications, 1992, pp. 55–79.
18. Jasper, J., *J. Phys. Chem. Ref. Data*, **1**[4] (1972) 938.
19. Mills, A. & MacKenzie, C., The application of bond parachors to organosilicon chemistry. *J. Am. Soc.*, **76** (1954) 2672–2673.
20. Bretsznajder, S., Prediction of transport and other physical properties of fluids. *Int. Series of Monographs in Chemical Engineering Vol. 11*, ed. P. Danckwerts. Pergamon Press, 1971.
21. Croix, O., Gounot, M., Bergez, P., Luce, M. & Cauchetier, M., Sintering of laser formed silicon carbide powders. In *Ceramics Today—Tomorrow's Ceramics*, ed. P. Vincenzini. Materials Science Monographs 66B, Elsevier, Amsterdam, The Netherlands, 1991, pp. 1447–1455.
22. Moenke, H. H. W., in *The Infrared Spectra of Minerals*. Mineralogical Society, London, 1974, p. 42.
23. Ocana, M., Fornes, V. & Serna, C. J., The variability of the infrared powder spectrum of amorphous SiO_2. *J. Non-Cryst. Solids*, **107**[2–3] (1989) 1892.
24. Bertoluzza, A., Fagnano, C., Morelli, M. A., Gottardi, V. & Gugliemi, M., Raman and infrared spectra on silica gel evolving towards glass. *J. Non-Cryst. Solids*, **48**[1] (1982) 117–128.
25. Cauchetier, M., Croix, O. & Luce, M., Laser synthesis of silicon carbide powders from silane and hydrocarbon mixtures. *Adv. Ceram. Mater.*, **3**[6] (1988) 548–552.
26. Scott, J. F. & Porto, S. P. S., Longitudinal and transverse optical lattice vibrations in quartz. *Phys. Rev. A.*, **161**[3] (1967) 903–910.
27. Sazaki, Y., Nishita, Y., Sato, M. & Okamura, K., Optical phonon states of SiC small particles studied by Raman scattering and infrared absorption. *Phys. Rev. B: Condens. Mater.*, **40**[3] (1989) 1762–1772.
28. Boulanger, L., Herlin, N., Luce, M., Cauchetier, M., Tougne, P., Hommel, H. & Legrand, A. P., Evolution of the structure of nanometric SiC laser-formed powders. In *Third Euro-Ceramics, Vol. 1*, Proceedings of the European Ceramic Society Third Conference (Madrid, Spain, 12–17 Sept. 1993), eds P. Duran and J. F. Fernandez. Faenza Editrice Iberica S.L., Madrid, Spain, 1993, pp. 21–26.
29. Mitomo, M. & Yoshioka, Y., Preparation of Si_3N_4 and AlN powders from alkoxide-derived oxides by carbothermal reduction and nitridation. *Adv. Ceram. Mater.*, **2**[3A] (1987) 253–256.
30. Tanaka, O. & Kurachi, Y., Synthesis of β-SiC powder from organic precursors and its sinterability. *Ceram. Int.*, **14**[2] (1988) 109–115.
31. White, D. A., Oleff, S. M. & Fox, J. R., Preparation of silicon carbide from organosilicon gels: II, Gel pyrolysis and SiC characterization. *Adv. Ceram. Mater.*, **2**[1] (1987) 53–59.
32. Kusabiraki, K., Infrared spectra of vitreous silica and sodium silicates containing titanium. *J. Non-Cryst. Solids*, **79**[1–2] (1986) 208–212.
33. Aizawa, M., Nosaka, Y. & Fujii, N., Preparation of TiO_2–SiO_2 glass via sol–gel process containing a large amount of chlorine. *J. Non-Cryst. Solids*, **168**[1–2] (1994) 49–55.
34. Miranda Salvado, I. M. & Fernandez Navarro, J. M., TiO_2–SiO_2 glasses prepared by the alkoxide route. *J. Non-Cryst. Solids*, **147 & 148** (1992) 256–261.
35. Miranda Salvado, I. M. & Fernandez Navarro, J. M., Al_2O_3–SiO_2 glassy materials prepared by the alkoxide route. pp. 1115–1120 in Vol. 2 of Ref. 28.
36. Komarneni, S., Roy, R., Selvaraj, U., Malla, P. B. & Breual, E., Nanocomposite aerogels: the SiO_2–Al_2O_3 system. *J. Mater. Res.*, **8**[12] (1993) 2343–2358.